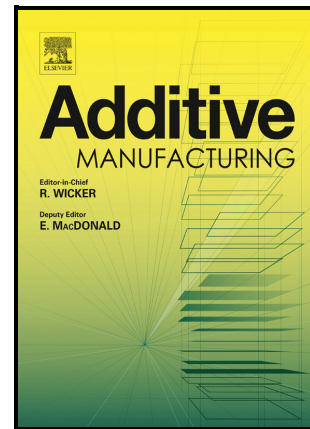


3D direct-write printing of water soluble micromoulds for high-resolution rapid prototyping

Saja Aabith, Richard Caulfield, Omid Akhlaghi, Anastasia Papadopoulou, Shervanthi Homer-Vanniasinkam, Manish K. Tiwari



PII: S2214-8604(22)00411-0

DOI: <https://doi.org/10.1016/j.addma.2022.103019>

Reference: ADDMA103019

To appear in: *Additive Manufacturing*

Received date: 17 March 2022

Revised date: 14 June 2022

Accepted date: 30 June 2022

Please cite this article as: Saja Aabith, Richard Caulfield, Omid Akhlaghi, Anastasia Papadopoulou, Shervanthi Homer-Vanniasinkam and Manish K. Tiwari, 3D direct-write printing of water soluble micromoulds for high-resolution rapid prototyping, *Additive Manufacturing*, (2022) doi:<https://doi.org/10.1016/j.addma.2022.103019>

This is a PDF file of an article that has undergone enhancements after acceptance, such as the addition of a cover page and metadata, and formatting for readability, but it is not yet the definitive version of record. This version will undergo additional copyediting, typesetting and review before it is published in its final form, but we are providing this version to give early visibility of the article. Please note that, during the production process, errors may be discovered which could affect the content, and all legal disclaimers that apply to the journal pertain.

# 3D direct-write printing of water soluble micromoulds for high-resolution rapid prototyping

*Saja Aabith<sup>1,2</sup>, Richard Caulfield<sup>1,2,3</sup>, Omid Akhlaghi<sup>1,2</sup>, Anastasia Papadopoulou<sup>1,2</sup>, Shervanthi Homer-Vanniasinkam<sup>2,4</sup>, Manish K. Tiwari<sup>1,2\*</sup>*

<sup>1</sup>Nanoengineered Systems Laboratory, UCL Mechanical Engineering, University College London, London, WC1E 7JE, U.K.

<sup>2</sup>Wellcome/EPSRC Centre for Interventional and Surgical Sciences, University College London, London, W1W 7TS, U.K.

<sup>3</sup>UCL Department of Medical Physics and Biomedical Engineering, University College London, London, WC1E 6BT, U.K.

<sup>4</sup>Leeds Vascular Institute, Leeds General Infirmary, Great George Street, Leeds LS1 3EX, UK

\*Corresponding author: m.tiwari@ucl.ac.uk

## Abstract

Direct-write printing has contributed tremendously to additive manufacturing; in particular extrusion based printing where it has extended the range of materials for 3D printing and thus enabled use across many more sectors. The printing inks for direct-write printing however, need a careful synthesis and invariably undergo extensive preparation before being able to be printed. This amounts to new ink synthesis efforts every time a new material is to be printed; which is particularly challenging for low storage modulus ( $G'$ ) materials like silicones, especially at higher resolutions (under  $10\ \mu\text{m}$ ). Here we report the development of a precise ( $< 10\ \mu\text{m}$ ) 3D printable polymer, with which we 3D print micromoulds, which are filled with standard silicones like polydimethylsiloxane (PDMS) and left to cure at room temperature. The proof of concept is demonstrated using a simple water soluble polymer as the mould material. The approach enables micrometre scale silicone structures to be prototyped with ease, away from the cleanroom.

## Keywords

High-resolution 3D printing, micromoulding, water based ink, precision prototyping, flexible/soft material prototyping

## 1. Introduction

The manufacturing world has taken big strides with the advent of additive manufacturing (AM) and 3D printing. There has been a surge of AM techniques that have been introduced within the last two decades alone, in particular, direct-write techniques [1] for small-scale manufacturing (<10  $\mu\text{m}$ ) [2]. Amongst these, the direct-write assembly approach pioneered by the Lewis group [3] in combination with the relevant material science exploitation of printable ink formulations [4] brought about excellent manufacturing control in various sectors including photonics [5,6], microfluidics [7], biomaterials [8], etc. [9] without requiring lithographic masks or similar expensive procedures [4]. However, each material to be deposited/printed with, needs much fine tuning of the ink properties such as viscosity [10], viscoelasticity [11], and evaporation rate [12] in order to be 3D printable and form self-standing structures. Additionally, at high resolution the ink would need to undergo further adjustments based on the surface/sample onto which it would be printed. This is due to the wide-ranging surface energies that are associated with different types of surfaces, which play a critical part in ensuring appropriate spreading and good adhesion of the ink while printing [13]. The many variables involved in the ink optimisation make the process extensive and time consuming. This is further complicated for inks where the curing is unattainable without external interference of temperature, radiation, etc. Such inks can be tuned to get 2D printing, but extending this to achieve 3D printability is challenging since the consecutively printed layer relies on the previously printed layer to be cured in time. Silicones, fall under this umbrella. The capability to manufacture precise silicone structures effectively has been much sought after due to silicones wide use that spans from electrical insulations in microelectronics to medical grade implants, contact lenses and catheters in the medical world. This is due to silicones valuable properties including high heat resistance and low surface energy [14], good flexibility [15], low toxicity, etc. [16]. The range of applications could be further expanded with increased precision and control in sub-millimetre scale silicone fabrication [17], assuredly leading to silicone materials playing an unparalleled role in many important areas such as nanotechnology.

Yirmibesoglu et al. [18] developed an extrusion system that incorporates an active mixer [19] and a controlled heat treatment [20] for successfully 3D printing 2-part (base & curing agent) silicone material. However, their system relies on a convective heater fan temperature of 80 °C and a heated bed temperature of 50 °C for the successful printing and curing of the two-part silicone. The temperature dependence of the system limits its use and makes printing on temperature sensitive surfaces impossible. Additionally, the resolution of the printed structures is limited to the nozzle size of 1.3 mm.

Eggbeer et al. [21] evaluated direct and indirect AM for the fabrication of maxillofacial prostheses. The direct AM process involved 3D printing the body of the prosthesis with a soft acrylate based material and wrapping it with a thin layer of silicone. The indirect AM procedure consisted of 3D printing a mould for the nasal prosthesis and filling it with silicone. The mould made (indirect AM) prosthesis was found to be

clinically suitable and even rated to be better than conventionally fabricated prostheses. Similar 3D printing techniques like fuse deposition modelling (FDM), etc. have been used for 3D printing moulds for prosthetics [22], but they lack in printing resolution and ease in the demoulding process, especially for sub-millimetre scale moulding (micromoulding) [23]. Additionally, for the case of complex structures the moulds need to be fractured (potentially damaging the moulding) or even bleached away as demonstrated by Jung et al. [24] who 3D printed polycaprolactone (PCL) - gelatine scaffolds as moulds for cell culture studies with an alkaline soluble photopolymer resin and projection-based microstereolithography (pMSTL). However, the moulds had to get washed away with alkaline solution (0.5 M NaOH), which has a pH of 13.69, that is comparable to the pH of bleach, thus limiting the application range due to product safety considerations. Similarly, Therriault et al. [25] reported a similar indirect AM approach for fabricating microvascular networks. However, the print resolution was limited to the nozzle size of 200  $\mu\text{m}$ . Additionally, the printed scaffold required high temperatures (75  $^{\circ}\text{C}$ ) to get removed. More recently, Kim et al. [26] have reported a magnetic field assisted direct-write printing approach of a ferromagnetic loaded elastomer matrix. However, the approach is limited to a nozzle size of 200  $\mu\text{m}$  and the printed scaffold – made up of silicone catalyst and silica nanoparticle composite – requires an organic solvent like chloroform to dissolve it away. Multiple groups [27-29] have demonstrated micrometer mould printing using stereolithography (SLA) and digital light processing (DLP) techniques. However, in particular for mould printing, both approaches inherently suffer from challenges that the direct-write approach overcomes. SLA and DLP printing are relatively slow (often limited by slow photopolymerisation rates) [30], expensive (due to the photosensitive resin and the need of a laser source) [31] and especially for mould printing, they require careful tuning of printing angles, in order to achieve the highest resolution [27]. This can lead to the need for printing multiple moulds to achieve desirable precision. Inkjet printing limited by the need for careful rheology control to ensure droplet/filament break-up and particularly challenging for non-linear, viscoelastic inks such as those considered here.

Here, in order to overcome the above mentioned limitations of the direct-write approach, we report the development of a 3D printable water-based polymer ink which is 3D printed to give hollow structures – micromoulds - that are then filled with the target material, like silicones such as Polydimethylsiloxane (PDMS) or Ecoflex. The water-based ink is clearly safe and is introduced to emphasise the simplicity of the approach. The filled moulds were cured at the appropriate temperature relevant to the filler material and then simply washed away with few water droplets, leaving behind the cured moulding (*see Fig. 2.*). This approach decouples the extensive ink synthesis – the major challenge of the direct-write approach [32] – from 3D direct-write printability, thus enabling simplistic advanced control in micrometre scale silicone AM without any harmful solvents, all while outside a cleanroom. This arrangement paves the way for high level integration in many sectors (like the healthcare sector). In particular, sectors, where it is required to

manufacture/print specific silicone structures onto pre-existing platforms, without causing any damage to the underlying device, which may be expensive and/or delicate.

## 2. Materials and methods

### 2.1 Inks

All the inks that were used are known to be safe and biocompatible and were prepared outside the cleanroom. Polyvinylpyrrolidone (PVP) was purchased from Sigma Aldrich. The ink was prepared by dissolving PVP mol. wt. 360 kDa in deionised (DI) water via stirring at 60 rpm at room temperature over 6 days. The relatively mild stirring process nudges the linear PVP strands to organise themselves into bundles, which are held together by the water through hydrogen bonding to C=O on the pyrrolidone ring. This inter-strand hydrogen bonding is enabled by the free rotation of the pyrrolidone ring on the C-N bond [33]. The homogeneous solution so obtained is printable directly, with suitably chosen nozzle diameters, without any further control on chemistry. The PVP ink was prepared in varying concentrations from 10 to 40 wt% in order to create a suitable range for testing 3D printability. Here we define 3D printability as the ability to form stable printed structures. Two different silicones were used to fill the printed moulds. Firstly, polydimethylsiloxane (PDMS, Sylgard 184) was purchased from Fisher Scientific and prepared in the recommended ratio of 10 parts of silicone base to 1 part of curing agent (10:1). This was stirred for 3 minutes and then desiccated in a vacuum chamber for another 20 minutes in order to remove the trapped air bubbles inside the silicone mixture. Additionally, Ecoflex (Ecoflex series 00-10 to 00-50) was purchased from Bentley Advanced Materials. Ecoflex was prepared in the recommended ratio of 1 part A to 1 part B (1:1). This was stirred for 2 minutes and desiccated in the vacuum chamber for 10 minutes.

### 2.2 Rheology of PVP inks

The effect of the different PVP concentrations on the viscosity and viscoelasticity of the printing inks was rheologically studied using a rheometer (DHR-3, TA instruments). All tests were carried out at room temperature (controlled), with a sandblasted parallel plate geometry (40 mm) and a sample gap of 500  $\mu\text{m}$ . The sandblasted parallel plate geometry was used to avoid any apparent wall slip [34]. The inks were subjected to a flow ramp (steady-state response) and oscillatory amplitude sweep. The amplitude sweep was performed at a frequency of 1 Hz over a torque range of 0.1 to 10,000  $\mu\text{N m}$  at 5 points per decade.

### 2.3 Printing

The direct-write printing system essentially consists of four main components: the nozzle assembly, the stage controllers (PC controlled) that control the three micro-translation stages (x, y and z; each with a motion step size of 50 nm and repeatability of 100 nm), an optical microscope focusing on the aperture of the nozzle and a nitrogen gas supply in combination with an electronic pneumatic regulator for applying set

pressures to the syringe barrel to force the ink out of the nozzle. The nozzle assembly comprises a syringe barrel that is filled with the required ink to be printed, a piston and an attached glass nozzle, which can be thought of as the ‘pen’ of the setup. The glass nozzles were fabricated using a micropipette puller (Sutter instrument, P-1000) providing varied apertures that can be as low as 600 nm. The nozzle aperture was determined based on the target application/resolution. The micro-translation stages (Physik Instrumente, M-111.12S) have a step resolution of 50 nm, a working range of 15 mm and a max velocity of 1 mm/s. The three stepper motor controllers (Physik Instrumente, model: C-663) were controlled via software (Physik Instrumente, PIMikroMove) and our LabVIEW (National Instruments) script. It should be noted that another setup with a higher step resolution of 1 nm was also used instead of the micro-translation stages. This was a piezoelectric actuated nanopositioning stage (Physik Instrumente, P-615.3CL Nanocube) with a step resolution of 1 nm and a working range of 350  $\mu\text{m}$  x 350  $\mu\text{m}$  x 250  $\mu\text{m}$ . The higher step resolution of the piezoelectric stage ensured smoother curvatures when printing curved moulds. The print quality and resolution were primarily controlled by carefully tuning the rheological properties (viscosity and viscoelasticity) of the inks to be printed with, the printing speed of the micro-translation stages and the surface wetting behaviour of the sample to be printed on top of (*see Fig. 1.*). The substrate wettability was not characterised specifically because we only used high-energy (wetable) substrates such as glass, copper, aluminium and stainless steel to ensure good adhesion of printed structures with the substrate. A proper investigation of the role of substrate wettability is beyond the scope of the current work and indeed will require a focussed investigation. However, substrates were cleaned in acetone and isopropanol to remove any contaminations. No attempt was made to alter surface through surface roughening or changing surface energy (wettability) through functionalisation or plasma treatment. The addition of polyvinylpyrrolidone to water (i.e. our inks) should have lower surface tension [35] and should facilitate better wettability/adhesion.

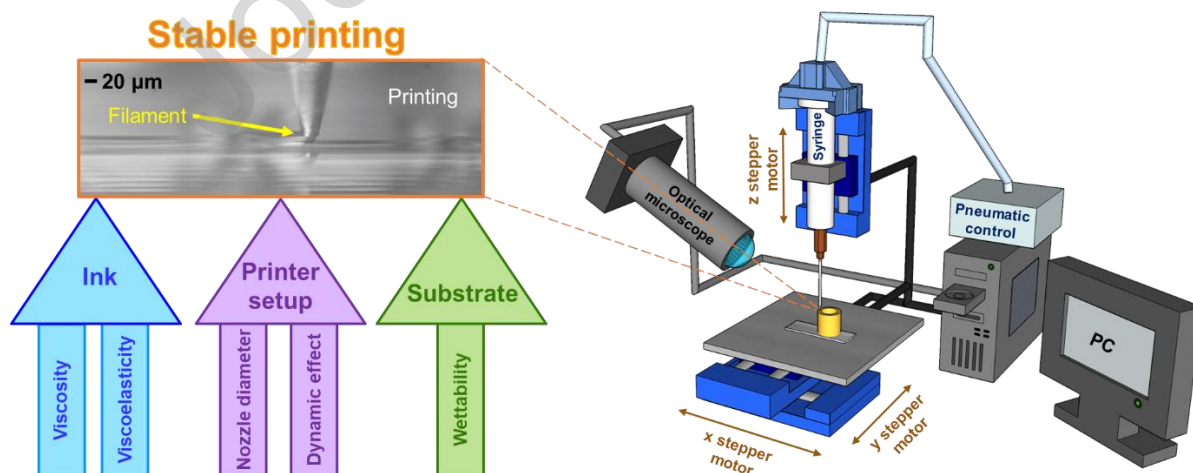


Fig. 1. Schematic of the direct-write assembly approach printing setup and printing variables influencing resolution and print quality



## 2.4 Micromould printing - decoupling ink synthesis and printability from rapid prototyping

For the mould fabrication, hollow 3D structures were printed with our developed PVP inks at a speed of 0.2 mm/s and nozzle apertures ranging from 5 to 35  $\mu\text{m}$  (see Fig. 2a. and Supplementary Video 1). The printed structures were then filled with PDMS, Ecoflex or composites like PDMS with carbon black nanoparticles. This was done by loading a syringe barrel with the desiccated silicone, attaching a 1 to 5  $\mu\text{m}$  nozzle to the syringe, lowering and aligning the nozzle assembly above the printed mould, the operator applying sufficient pressure (0.1 to 0.3 bar) to the piston to just force the filler ink out of the nozzle and retracting the nozzle assembly once the mould was filled to the brim (see Fig. 2b.). The mould was considered to be 'filled to the brim' when the inner edge of the mould was not visible. All steps of which were completely observable via the optical microscope that was tilted at 45° (see Fig. S1. and Supplementary Video 2). The filled mould was left to cure in an oven at 125 °C for 20 minutes or at room temperature for 48 hours, such that the PDMS cured completely (see Fig. 2c.). The mould with the cured moulding was placed outside the oven at RT for another 10 minutes to cool down completely. The water soluble PVP mould was then easily washed away with a few water droplets by simply pipetting water droplets onto the mould, resulting in the moulding (PDMS structure) to remain behind (see Fig. 2d.). This was done for different structures including 3D hexagons (see Fig. 2i-iv.).

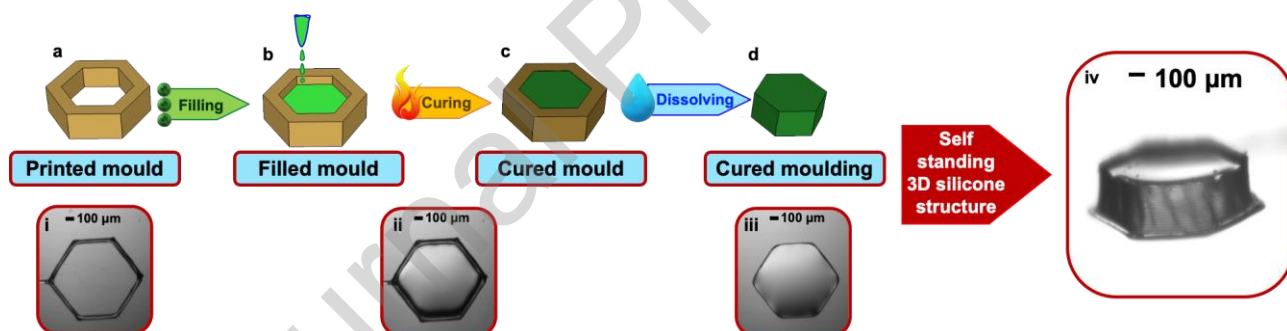


Fig. 2. Mould process: a.) Printing PVP mould b.) Filling printed mould with PDMS via nozzle c.) Curing mould with PDMS content at RT for 48 hours or in an oven at 125 °C for 20 minutes d.) Pipetting few water droplets onto the mould in order to dissolve PVP moulding and leaving behind cured and structured PDMS i.) Printed hexagonal structure ii.) PDMS filled and cured mould iii.) top view of cured moulding without mould iv.) 3D view of cured moulding without mould

## 3. Results & Discussion

### 3.1 Rheology of PVP inks

The flow behaviour and viscoelastic properties for 10, 15, 20, 25 and 30 wt% PVP ink concentrations were obtained. From the steady-state response (see Fig. 3a.), the zero shear viscosity values increase from 0.3 Pa.s to 40 Pa.s with increase in PVP concentration. The inks show clear shear thinning across the PVP concentrations in the shear rate ( $\dot{\gamma}$ ) region of 46 – 1600  $\text{s}^{-1}$ , which corresponds to our printing speed of 0.2

mm/s for nozzle sizes 1 – 35  $\mu\text{m}$ ; calculated using  $\dot{\gamma}_{max} = 4\dot{Q}/\pi r^3$ , where  $r$  is the nozzle radius and  $\dot{Q}$  is the volume flow rate, which is calculated as  $\dot{Q} = V_p \pi r^2$  with  $V_p$  being the printing speed [36]. The higher concentration inks (20 to 30 wt%) show small shear thickening for the lower shear rates, which can be attributed to the intermolecular entanglements which can form during low shear rates [37]. These entanglements will get destroyed during the higher shear rates, leading to the reduced viscosity (shear thinning). The developed inks showed no thixotropic behaviour. This was determined by looking for hysteresis in another flow ramp test (ramp up and down), which was applied on 10 wt% and 25 wt% inks. Viscosity as a function of shear rate was shown (see Fig. S2.), where the ramp up and down data points overlapped, suggesting no hysteresis behaviour. The non-thixotropic behaviour of the inks was further ascertained by a 3 step test (see Fig. S3.), where a low shear rate of  $1 \text{ s}^{-1}$  was applied for 10 s, followed by applying an increased shear rate of  $100 \text{ s}^{-1}$  for 10 s and then in the third step reducing the shear rate to  $1 \text{ s}^{-1}$  for another 10 s. There was no time delay visible and the viscosity followed the shear rate instantaneously.

The flow index numbers ( $n$ ) for the different PVP concentrations (see Fig. 3c.) were obtained from least square fitting a power law model  $\tau = \alpha \dot{\gamma}^n$  to the shear stress ( $\tau$ ) as a function of shear rate ( $\dot{\gamma}$ ), where  $\alpha$  is the slope (see Fig. 3b.). The flow index numbers for the different PVP concentrations are very similar, ranging from 0.64 to 0.75. These similar flow index values suggest similar flow behaviour across all of the different PVP concentrations tested.

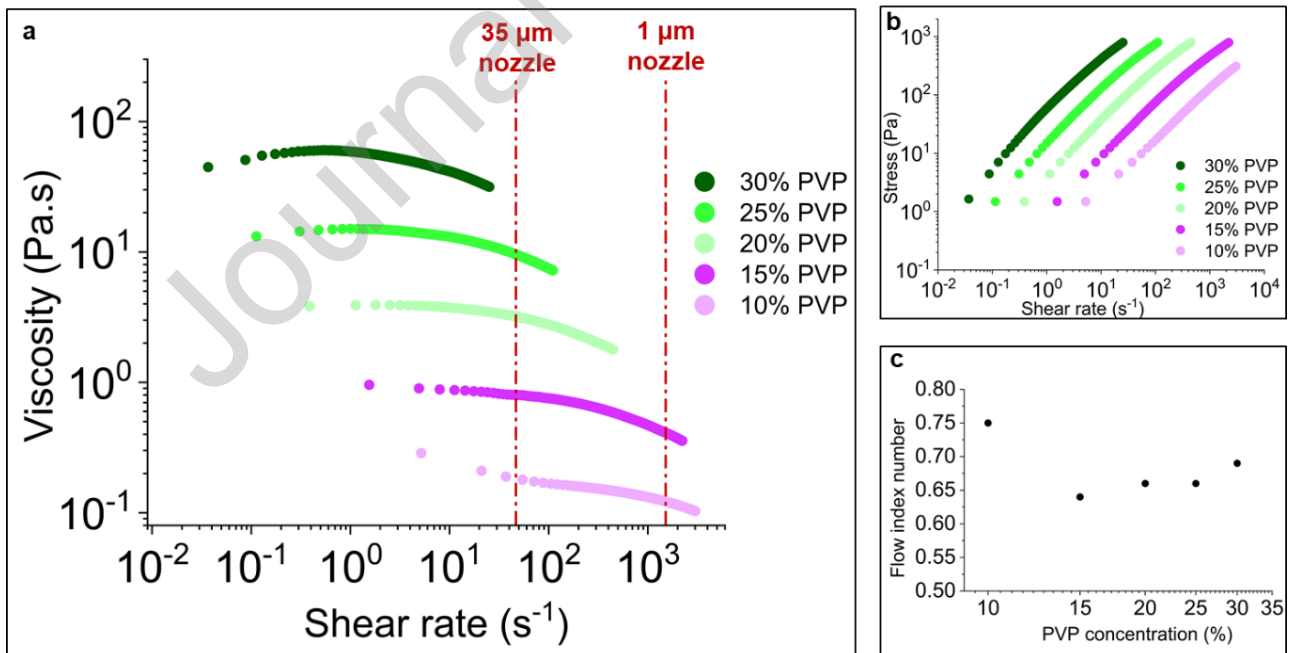


Figure 3: Steady-state response of PVP inks: a.) Viscosity as a function of shear rate b.) Oscillation stress as a function of shear rate c.) Flow index number for PVP ink concentrations

The viscoelastic response (see Fig. 4a.) shows that the storage modulus is lower than the loss modulus for all PVP concentrations ( $G' < G''$ ). This agrees with the findings of Guo et al. who used UV assisted 3D



printable polyimide ink [38]. However, it is in contrast to the 3D printable graphene oxide (GO) based inks from García-Tuñón et al. [39] and the 3D printable silver flake loaded thermoplastic polyurethane (AgTPU) from Valentine et al. [40], both of which have a higher storage modulus than loss modulus ( $G' > G''$ ).

Determining the dominant modulus is important as this feature has an influence on the ink consistency and print resolution (see Fig. 4b.): the GO based ink and the AgTPU ink are more paste like and are printed with 510  $\mu\text{m}$  and 200  $\mu\text{m}$  nozzles respectively, which is bigger than the 90  $\mu\text{m}$  nozzles used for the polyimide ink, as it was more liquid-like and also needed UV assistance while printing to help the curing/printing process. It should be noted that the biggest nozzle size that was used in our work was 35  $\mu\text{m}$ , without any UV cure assistance.

As for the inks that have been developed in this work, despite  $G''$  being greater than  $G'$ , stable structures were successfully printed thanks to the evaporation of the solvent (water). The evaporation became stronger with reduction in nozzle size, such that the evaporation time  $\tau_v \sim d^2$ , where  $d$  is the filament diameter. However, it should be also noted that evaporation also has a negative impact of causing nozzle clogging, particularly for finer nozzles.

The  $G''/G'$  plot in Figure 4b shows the expected outcome of the liquid-like inks approaching the gelation point ( $G' = G''$ ) [41] when increasing the polymer content of the ink. This is due to the increased formation of polymer networks when the polymer content is increased.

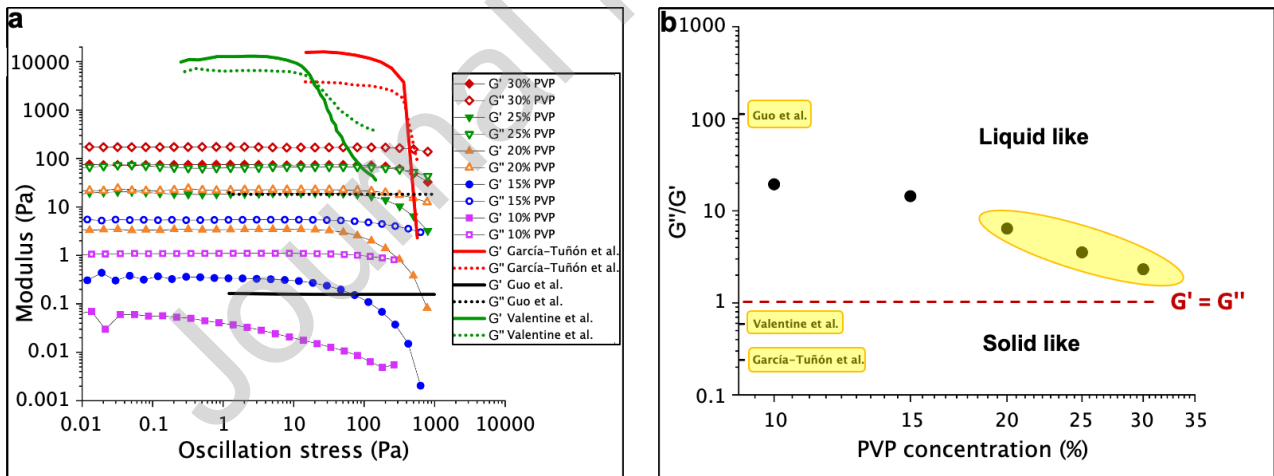


Fig. 4. Viscoelastic properties of PVP inks: a.)  $G'$  and  $G''$  as a function of oscillation stress for the different PVP concentrations and other reported inks [38-40] b.) Ratio of loss modulus to storage modulus as a function of PVP concentration in comparison to other inks [38-40], with the 3D printable inks highlighted in yellow

### 3.2 Printability of PVP inks

In order to develop a 3D printable water based PVP ink, the PVP concentration was varied from 10 to 40 wt% and tested with different nozzle (tip) apertures ranging from 1  $\mu\text{m}$  to 35  $\mu\text{m}$ . The 40 wt% PVP ink was

unprintable and always led to nozzle clogging. By 'nozzle clogging' we mean that the ink stops flowing through the nozzle due to one of two reasons. The first reason applies for the 40 or more wt% PVP inks only, where the ink was too viscous so that it could not flow through the nozzle. The second reason was due to the opening (aperture) of the nozzle getting slowly blocked by PVP ink that accumulated over the printing duration, which mostly occurred for the smaller ( $<5\ \mu\text{m}$ ) nozzles. This indeed also highlights the challenges faced in direct-write printing at such resolutions.

Figure 5 summarises the printability of the different PVP concentration inks with respect to nozzle sizes. It should be noted that the micropipette puller machine fabricated varying nozzle sizes, which resulted in the implementation of a nozzle size bin classification. However the data points (1-3, 10, 20 and  $30\ \mu\text{m}$ ) in figure 5 were the actual sizes of the nozzles that were frequently printed with ( $>5$  print runs each). The rest of the nozzle sizes within each classification were test printed with fewer times than the data point nozzle sizes.

With nozzle sizes of  $35\ \mu\text{m}$  to  $15\ \mu\text{m}$  and a PVP concentration of 30 wt%, 'multilayer printing' - the ink was 3D printable and able to form self-standing structures without the nozzle clogging or fracturing at consecutive layers - was achieved (see Fig. 5d.). Being able to 3D print multiple layers is crucial for making fully formed 3D structures. 'Multilayer printing' was also achievable with nozzle sizes of  $25\ \mu\text{m}$  to  $15\ \mu\text{m}$  and PVP concentration of 25 wt%. Similarly, multilayer printing was attained with nozzle sizes of  $15\ \mu\text{m}$  to  $5\ \mu\text{m}$  and the 20 wt% PVP ink.

It should be noted that the extruded filament did show die swelling effect after exiting the nozzle [42]. Additionally filament wetting may reduce the final dried up height of the extruded filament on the substrate. The amount of wetting was different for different substrates (different surface energies), but based on our print runs, the wetting on glass substrate causes the filament width to be  $\sim 1.5\times$  the nozzle aperture. So that for a  $10\ \mu\text{m}$  nozzle, the extruded filament would be  $\sim 15\ \mu\text{m}$  wide and  $\sim 10\ \mu\text{m}$  high on the substrate. These dimensions were highly reproducible for given ink PVP concentration and nozzle size. This enabled us to build vertical structures while keeping the vertical increment for each layer constant. So that for printing a  $100\ \mu\text{m}$  high structure with a  $10\ \mu\text{m}$  nozzle, the stages are programmed such that they increment  $10\ \mu\text{m}$  after each layer for 10 layers. The approach was successfully exploited to build multi-layered structures without the nozzle losing fluid contact in one of the consecutive print layers (see Fig. 54). For all PVP concentrations, using nozzles under  $5\ \mu\text{m}$  only enabled 'single layer printing'. Single layer printing meaning being able to print a single complete layer, after which the nozzle either clogs up or breaks (see Fig. 5c.).

The 10 wt% PVP ink with nozzle sizes of  $35\ \mu\text{m}$  to  $15\ \mu\text{m}$  was not printable. In this case, the ink simply wet the surface without forming a filament (see Fig. 5a.). Nozzle sizes less than  $14\ \mu\text{m}$  but bigger than  $3\ \mu\text{m}$  were 'printable' with the 10 wt% PVP ink - being able to form filaments that are adhering to the surface,

but not being able to complete the first layer due to either nozzle fracturing, clogging up or the ink overflowing (see Fig. 5b.).

As shown in Figure 4 all of our inks are liquid-like and approaching the gelation point with increase in polymer content. However, among the printable inks, from the least liquid like 30 wt% PVP ink to the most liquid-like 10 wt% PVP ink we developed, we could not achieve multilayer printing with nozzle sizes that were smaller than 5  $\mu\text{m}$ , which broke frequently. This suggests that despite having dominating  $G''$  and sufficient  $G'$  to form filaments, the stability of the glass nozzles is more of a dominating factor to achieve multilayer printability, since a low  $G'$  is sufficient to break the fine glass nozzles and hinder continuous printability to achieve multilayer printing. If the glass nozzles under 5  $\mu\text{m}$  were made with a material of sufficiently high strength, then multilayer printing could be achievable for all the nozzle apertures and their respective ink concentrations in the shaded region in Fig. 5. However, in order to verify this another study that uses other glass tips that have sufficiently higher Young's modulus to overcome the stress applied by the inks should be conducted. Yuk and Zhao [43] developed a quantitative phase diagram to map different printing modes for viscoelastic inks (see Fig. S5). The phase diagram maps different printing modes of viscoelastic inks with the help of non-dimensional parameters ( $H^*$ ,  $V^*$ ), where  $H^*=H/\alpha D$  and  $V^*=V/C$ , with  $H$  being the gap between the tip and the substrate,  $\alpha$  being the die-swelling ratio,  $D$  being the diameter of the tip,  $V$  being the tip moving speed and  $C$  being the extrusion rate. Our developed water based PVP inks all die-swell upon extrusion ( $V^*\geq 1$ ) and  $H^*=0.41$  ( $H=0.5*D$ ,  $\alpha=1.23$ , see Fig. S5a.). The phase diagram doesn't cater for  $H^*<1$ . Separately, the phase diagram doesn't take into consideration mechanical failure of the nozzles, since the group uses metal tips that have apertures of  $\geq 50 \mu\text{m}$  and inks that are solid-like ( $G''/G' < 1$ ). But in our work we are working with much smaller nozzle apertures (1 to 35  $\mu\text{m}$ ) that are made of fragile glass capillaries that can break due to ink accumulation or clogging and our inks are liquid-like ( $G''/G' > 1$ ). This is the reason why our plot is more suitable for our printing conditions, where mechanical failure of glass nozzles due to ink accumulation or clogging must be taken into account, since mechanical failure hinders printability.

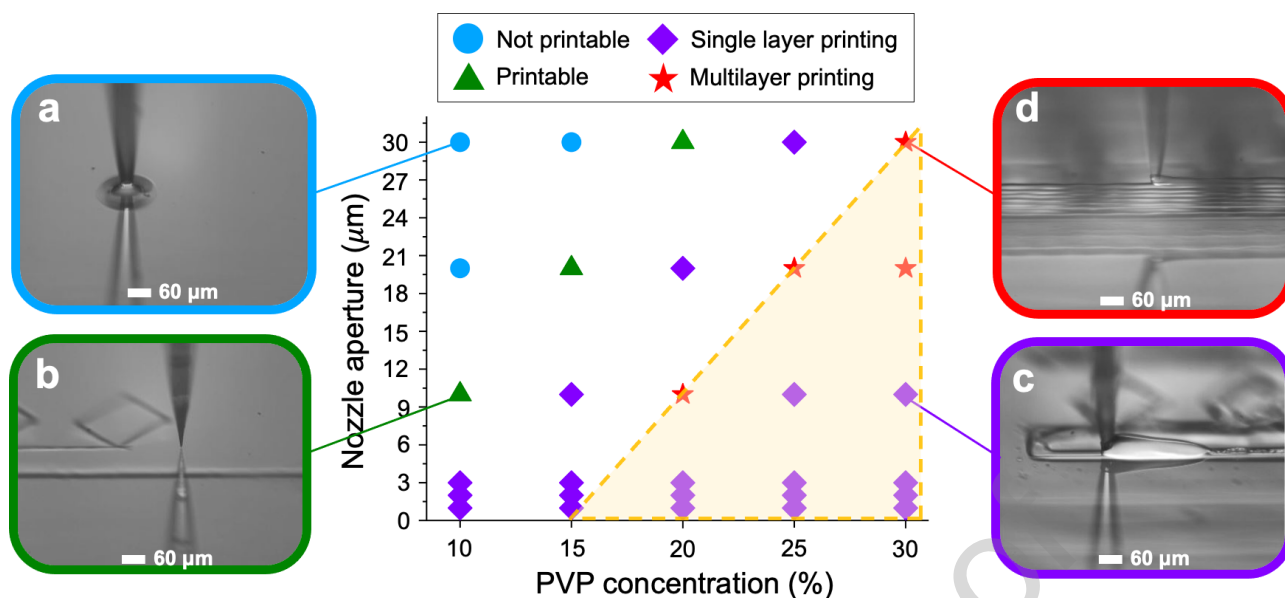


Fig. 5. Map of printability of the inks with different PVP concentrations with different nozzle sizes. Four regions are identified: a.) 'Not printable' meaning that the ink would just wet the substrate without forming a surface adhering filament b.) 'Printable' meaning that the ink facilitated filament formation that adhered to the surface, but unable to complete the initial layer due to either nozzle fracture, clogging or overflowing c.) 'Single layer printing' meaning printing could be completed for a single layer, but unable to proceed to multiple layers due to nozzle clogging or fracture d.) 'Multilayer printing' meaning that the ink was 3D printable and enabled the formation of stable/self-standing structures without the nozzle clogging or fracturing at consecutive layers. Shaded region represents the multilayer printing region if nozzle stability was not a factor.

### 3.3 Moulding and prototyping

The micromoulds were successfully printed onto various substrates including glass, copper, aluminium and stainless steel, owing to the good adhesion properties of PVP. The printable substrate range extends the potential applications of this moulding approach further.

Some of the moulds that were printed and their corresponding mouldings are shown in Figure 6. The star shape logo of UCL's Wellcome/EPSRC centre for Interventional and Surgical Sciences (WEISS) was printed on glass with a 10  $\mu\text{m}$  nozzle and 25 wt% PVP ink. The WEISS logo was printed at a velocity of 0.2 mm/s, so that the whole printout took 37 seconds. The printed logo was consecutively filled with PDMS 10:1 (see Fig. 6a.). The printed mould was only 1 layer high ( $\sim 10 \mu\text{m}$ ), thus showing how suitable a water-based mould is in getting filled with a hydrophobic filling (PDMS). The hydrophobicity of the PDMS stops it from crossing the printed mould boundaries.

The concentric rings were printed with a 10  $\mu\text{m}$  nozzle and 20 wt% PVP ink to create a multi-layer design of height 20  $\mu\text{m}$  (see Fig. 6b.(i, ii)). The gaps of the concentric rings were filled with PDMS in an alternating manner, i.e. the first filling would be at gap 1 (centre), then gap 3 and then finally gap 5. This was to demonstrate the micrometer precision control in the filling process. Then the PDMS was cured as before.

The supporting mould was then washed away, leaving behind 3 concentric PDMS rings. Following the procedure outlined by Goyal et al. [44] the PDMS rings were then submerged in a gold salt solution for 24 hours. The platinum curing agent in the Sylgard 184 PDMS catalyses the reduction of the gold salt *in situ* to give gold nanoparticles, which embed themselves into the PDMS structure (see Fig. 6b.(iii)). This is a facile method of synthesising gold nanoparticle - PDMS composites, such composite materials have uses in optical and photoacoustic sensing applications [45]. Here it serves as a means to demonstrate the versatility of our approach to create reactive components leading *in situ* nanoparticle formation, thereby facilitating soft nanocomposite formation.”

Similarly, more complex 3D structures like pyramids and hourglasses were printed. A pyramidal mould was printed with a 15  $\mu\text{m}$  nozzle and 30 wt% PVP ink (see Fig. 6c.(i, ii)). The Ecoflex moulding is of good quality, where the number of layers can be seen from the moulding itself. The tip of the pyramid is under 50  $\mu\text{m}$  in diameter (see Fig. 6c.(iii)). Additionally, an hourglass shaped mould was printed with a 10  $\mu\text{m}$  nozzle and 20 wt% PVP ink with the higher resolution printing setup at a reduced speed of 0.04 mm/s to avoid stringing on the curved structure. The complete hourglass printout took 4 minutes and 24 seconds. The mould was filled with PDMS, then cured and demoulded as before. The hourglass mould (see Fig. 6d.(ii)), is a smaller mould than the other moulds (Fig. 6a-c.(ii)), and thus minor defects, such as the small strand that is formed when retracting the nozzle after the mould printing can affect the quality of the moulding. However, the extra string of PVP that was formed while retracting the nozzle after printing (see Fig. 6d.(ii)), was washed away in the demoulding process (see Fig. 6d.(iii)).

Following this procedure, we highlight how silicone microstructures manufactured using our technique can be utilised to create functional nanocomposite materials across many different areas, either directly or as an initial step in a more complex manufacturing process. It should be noted that the overall manufacturing time of our approach is only a fraction of the manufacturing time of other high-resolution manufacturing approaches, that are predominantly subtractive approaches. To achieve 10  $\mu\text{m}$  repeatability in a typical photolithographic process would comprise of multiple challenging steps to obtain just a soft lithographic pattern, which could take almost 2 days. However, our approach achieves this within minutes.

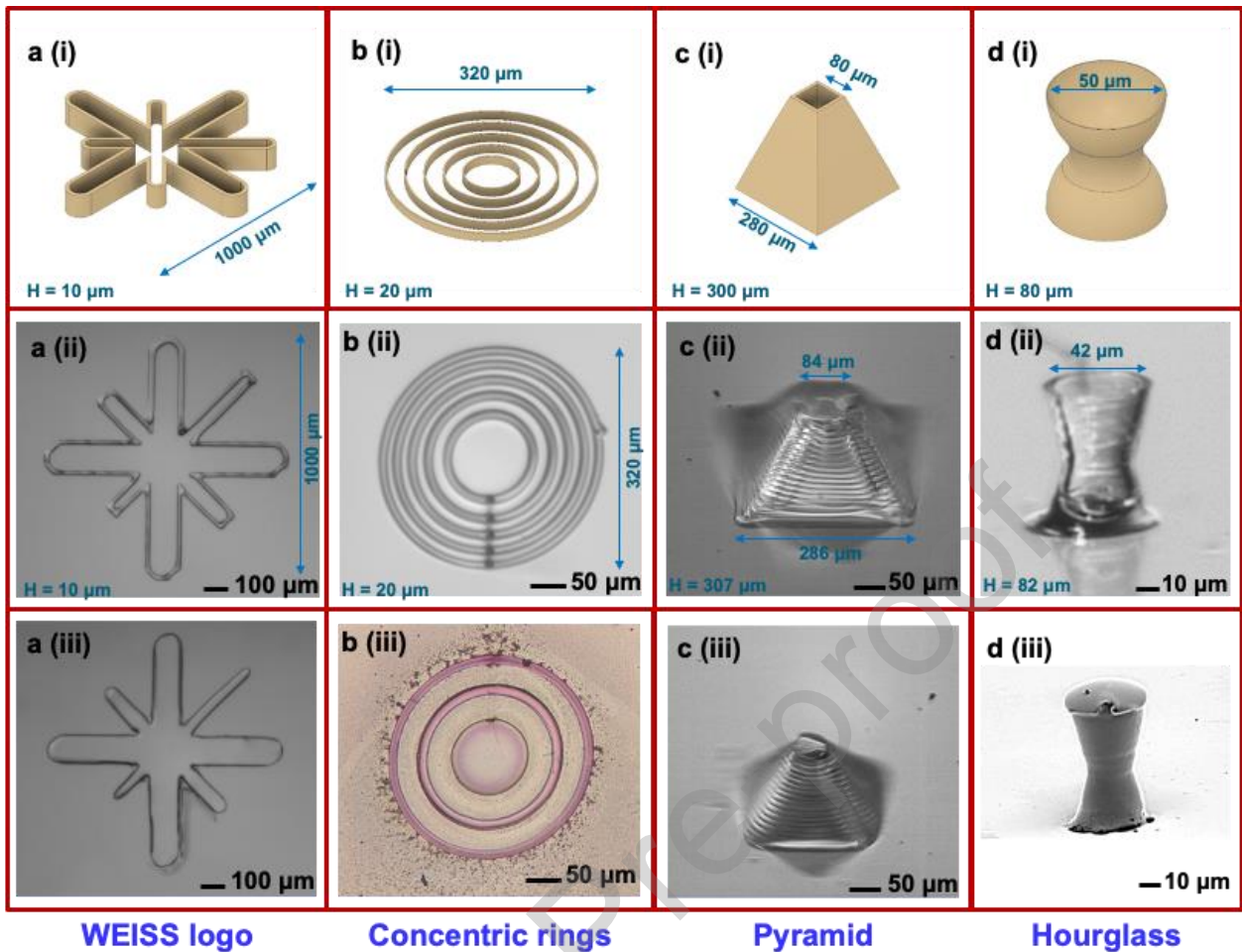


*Fig. 6. Printed moulds and their mouldings: a.) (i) WEISS (Wellcome/EPSCRC Centre for Interventional and Surgical Sciences) logo mould schematic, (ii) printed mould and (iii) PDMS moulding b.) (i) Concentric rings mould schematic, (ii) printed mould and (iii) moulding of PDMS with embedded gold nanoparticles c.) (i) Pyramidal structure mould schematic, (ii) printed mould and (iii) moulding of Ecoflex d.) (i) Hourglass mould schematic, (ii) printed mould and (iii) moulding of PDMS*

Still, there are some limitations that need to be overcome in order to enhance our approach even further. Moulding a scaffold like a truss structure or a woodpile structure would be challenging with our approach. However, soft lithography could serve as a potential workaround for some challenging structures like the woodpile structure, where the negative of the mould – closely spaced cubes with a surrounding wall – would be printed with PVP and moulded with PDMS. This way a PDMS master is obtained (PDMS soft mould). This can be vapour treated with trichlorosilane for easy demoulding [46]. The treated PDMS soft mould can be used to mould a PDMS woodpile structure. Additionally, the printed moulds leave behind sub-micron sized indents of the layers on the moulding, which can be a limitation for certain applications like microlenses.

To put our work in the context, *Fig. 6.* clearly shows the potential of our approach to prototype otherwise difficult to structure materials like PDMS. Although, a thorough investigation of the printing fidelity and precise obtainable resolutions are beyond the scope of the current work, some general inferences can be drawn. As such, the printing fidelity depends on three different features:



- (i) accuracy of the positioning system used,
- (ii) the difference between the nozzle size and the extruded filament diameter (which depends on the die-swell ratio and the substrate/inter-layer wettabilities of printed filament)
- (iii) and the mechanical stability of the printed structure.

As mentioned above, the positioning system that we have employed has the coarsest repeatability of 100 nm; we also used a system with sub-nm position repeatability. Therefore this is likely to have small effect on the accuracy.

As mentioned before, we found that the extruded filament height was the same as the nozzle diameter and the extruded filament width was consistently  $\sim 1.5$  x the nozzle diameter. Lastly, we observed no changes in the diameter of the printed PVP filaments and the shrinkage of the PDMS is known to be ca. 1% (47). There are noticeable differences in the dimensions between the design and the final prototype dimensions. For example, in the hourglass case, the design diameter of the top of the hourglass was 50  $\mu\text{m}$  and the corresponding diameter on the mould was 42  $\mu\text{m}$ . This is due to material (ink) overflow. Note that this overflow is very limited when the aspect ratio of the printed structure is small. Overall, this leads to ca. 2% lower dimensions for first few layers of printing (compared to the design dimension) and goes to ca. 40% for the highest aspect ratio such as the pyramid (see Fig. 6c.) and hourglass (see Fig. 6d.).

It is also important to note that with our PVP based moulds it is not possible to remove the filament traces after printing. However, we can reduce the imprint size by using a translating stage with finer step precision, just as we did for the hourglass in Fig. 6d., where the imprints are hardly visible. Melt processable polymers may possibly allow a complete smoothing of the imprints. However, they are beyond the scope of the current work and PDMS is known to faithfully replicate geometries as high as few nm precision (48).

#### 4. Conclusion

To facilitate precision prototyping of silicones as an exemplar material, using high-resolution 3D direct-writing, we developed and rheologically characterised a set of water soluble PVP inks. These PVP inks facilitated rapid high-resolution prototyping, enabling micrometer structures to be fabricated with ease outside of any cleanroom environment which is typically required for such high-resolution manufacture (e.g. for mould manufacture). A number of exemplar micromould geometries were printed using this approach and silicone and silicone nanocomposite structures were successfully demonstrated. The study and the approach introduces a safe and simple approach to prototype high-resolution ( $<10$   $\mu\text{m}$ ) structures using direct-write 3D printing, without the need for exhaustive formulation and optimisation of inks. This tends to be a major challenge because often the material with suitable properties for a desirable application lacks the features to be 3D printed. Although, our demonstrations concentrate on silicones (that lacked the required viscoelastic features to be printed directly), the freedom gained from removing the need for painstaking ink optimisation process will open the door to a variety of soft, 3D microstructures

prototyping for a wide range of applications in areas such as flexible electronics (i.e. sensors) and bioengineering (i.e. implants, etc.).

#### **Acknowledgement:**

Partial support from the Wellcome/EPSRC Centre for Interventional and Surgical Sciences (WEISS) (203145Z/16/Z), European Research Council (ERC) under the European Union's Horizon 2020 research and innovation programme under grant agreement no. 714712 and EPSRC DTP studentship award.

#### **5. References**

- [1] L. Mortara, J. Hughes, P.S. Ramsundar, F. Livesey, D.R. Probert, Proposed classification scheme for direct writing technologies, *Rapid Prototyp. J.* 15 (2009) 299–309. doi:10.1108/13552540910979811.
- [2] F. Feihuang and S. Aabith, S. Homer-Vanniasinkam, M.K. Tiwari, High-resolution 3D printing for healthcare underpinned by small-scale fluidics, 2017. doi:10.1016/B978-0-08-100717-4.00023-5.
- [3] J. Lewis, Colloidal processing of ceramics and composites, *J. Am. Ceram. Soc.* 83 (2000). doi:10.1179/1743676111Y.0000000075.
- [4] J.A. Lewis, G.M. Gratson, Direct writing in three dimensions, *Mater. Today.* (2004). doi:10.1016/S1369-7021(04)00344-X.
- [5] G.M. Gratson, F. García-Santamaría, V. Lousse, M. Xu, S. Fan, J.A. Lewis, P. V. Braun, Direct-write assembly of three-dimensional photonic crystals: Conversion of polymer scaffolds to silicon hollow-woodpile structures, *Adv. Mater.* (2006). doi:10.1002/adma.200501447.
- [6] P.I. Dietrich, M. Blaicher, I. Reuter, M. Billah, T. Hoose, A. Hofmann, C. Caer, R. Dangel, B. Offrein, U. Troppenz, M. Moehrle, W. Freude, C. Koos, In situ 3D nanoprinting of free-form coupling elements for hybrid photonic integration, *Nat. Photonics.* (2018). doi:10.1038/s41566-018-0133-4.
- [7] S. Ghorbanian, M.A. Qasaimeh, M. Akbari, A. Tamayol, D. Juncker, Microfluidic direct writer with integrated declogging mechanism for fabricating cell-laden hydrogel constructs, *Biomed. Microdevices.* (2014). doi:10.1007/s10544-014-9842-8.
- [8] J. Ma, Y. Wang, J. Liu, Bioprinting of 3D tissues/organs combined with microfluidics, *RSC Adv.* (2018). doi:10.1039/c8ra03022g.
- [9] J.A. Lewis, Direct ink writing of 3D functional materials, *Adv. Funct. Mater.* (2006).

doi:10.1002/adfm.200600434.

- [10] G.K. Batchelor, *An introduction to the fluid dynamics*, (1967).
- [11] E.B. Duoss, T.H. Weisgraber, K. Hearon, C. Zhu, W. Small IV, T.R. Metz, J.J. Vericella, H.D. Barth, J.D. Kuntz, R.S. Maxwell, C.M. Spadaccini, T.S. Wilson, Three-dimensional printing of elastomeric, cellular architectures with negative stiffness, *Adv. Funct. Mater.* (2014). doi:10.1002/adfm.201400451.
- [12] G. McHale, S.M. Rowan, M.I. Newton, M.K. Banerjee, Evaporation and the Wetting of a Low-Energy Solid Surface, *J. Phys. Chem. B.* (1998). doi:10.1021/jp972552i.
- [13] W.A. ZISMAN, Relation of the Equilibrium Contact Angle to Liquid and Solid Constitution, in: 1964. doi:10.1021/ba-1964-0043.ch001.
- [14] B.P. and J.W.W. T.C. Kendrick, Siloxane polymers and copolymers, in: *Chem. Org. Silicon Compd.*, 1989: p. 1292.
- [15] D.C.E.S. X. Thomas, *Silicones in Medical Applications*.
- [16] K. Mojsiewicz-Pienkowska, M. Jamrógiewicz, K. Szymkowska, D. Krenczkowska, Direct human contact with siloxanes (silicones) - safety or risk part 1. Characteristics of siloxanes (silicones), *Front. Pharmacol.* (2016). doi:10.3389/fphar.2016.00132.
- [17] J. Chojnowski, M. Cypryk, Synthesis of Linear Polysiloxanes, in: R.G. Jones, W. Ando, J. Chojnowski (Eds.), *Silicon-Containing Polym. Sci. Technol. Their Synth. Appl.*, Springer Netherlands, Dordrecht, 2000: pp. 3–41. doi:10.1007/978-94-011-3939-7\_1.
- [18] O.D. Yirmibesoglu, J. Morrow, S. Walker, W. Gosrich, R. Canizares, H. Kim, U. Daalkhaijav, C. Fleming, C. Branyan, Y. Menguc, Direct 3D printing of silicone elastomer soft robots and their performance comparison with molded counterparts, *2018 IEEE Int. Conf. Soft Robot. RoboSoft 2018.* (2018) 295–302. doi:10.1109/ROBOSOFT.2018.8404935.
- [19] T.J. Ober, D. Foresti, J.A. Lewis, Active mixing of complex fluids at the microscale, *Proc. Natl. Acad. Sci.* (2015). doi:10.1073/pnas.1509224112.
- [20] J. Morrow, S. Hemleben, Y. Menguc, Directly Fabricating Soft Robotic Actuators With an Open-Source 3-D Printer, *IEEE Robot. Autom. Lett.* (2017). doi:10.1109/LRA.2016.2598601.
- [21] D. Eggbeer, R. Bibb, P. Evans, L. Ji, Evaluation of direct and indirect additive manufacture of maxillofacial prostheses, *Proc. Inst. Mech. Eng. Part H J. Eng. Med.* 226 (2012) 718–728. doi:10.1177/0954411912451826.
- [22] F. Liravi, E. Toyserkani, Additive manufacturing of silicone structures: A review and prospective, *Addit. Manuf.* 24 (2018) 232–242. doi:10.1016/j.addma.2018.10.002.

- [23] V. Schulze, P. Weber, M. Deuchert, S. Haupt, C. Ruhs, A. Kienzler, Limits and challenges of manufacturing micro moulds, *Int. J. Nanomanuf.* 6 (2010) 176. doi:10.1504/ijnm.2010.034782.
- [24] J.W. Jung, H. Lee, J.M. Hong, J.H. Park, J.H. Shim, T.H. Choi, D.W. Cho, A new method of fabricating a blend scaffold using an indirect three-dimensional printing technique, *Biofabrication.* (2015). doi:10.1088/1758-5090/7/4/045003.
- [25] D. Therriault, R.F. Shepherd, S.R. White, J.A. Lewis, Fugitive inks for direct-write assembly of three-dimensional microvascular networks, *Adv. Mater.* 17 (2005) 395–399. doi:10.1002/adma.200400481.
- [26] Y. Kim, H. Yuk, R. Zhao, S.A. Chester, X. Zhao, Printing ferromagnetic domains for untethered fast-transforming soft materials, *Nature.* 558 (2018) 274–279. doi:10.1038/s41586-018-0185-0.
- [27] S. Choo, S. Jin, J. Jung, (2022) Fabricating High-Resolution and High-Dimensional Microneedle Mold through the Resolution Improvement of Stereolithography 3D Printing. *Pharmaceutics*, 14, 766. <https://doi.org/10.3390/pharmaceutics14040766>
- [28] R. Wick-Joliat, M. Tschamper, R. Kontic, D. Penner, (2021) Water-soluble sacrificial 3D printed molds for fast prototyping in ceramic injection molding, *Additive Manufacturing*, Volume 48, Part B, 102408, ISSN 2214-8604, <https://doi.org/10.1016/j.addma.2021.102408>.
- [29] M. Hopkins, S. Gunbay, C. Hayes, V. F. Moritz, E. Fuenmayor, J. G. Lyons, D. M. Devine, (2021) Stereolithography (SLA) utilised to print injection mould tooling in order to evaluate thermal and mechanical properties of commercial polypropylene, *Procedia Manufacturing*, Volume 55, Pages 205-212, ISSN 2351-9789, <https://doi.org/10.1016/j.promfg.2021.10.029>
- [30] J. Z. Manapat, Q. Chen, P. Ye, R.C. Advincula, *Macromol. Mater. Eng.* (2017), 302, 1600553. <https://doi.org/10.1002/mame.201600553>
- [31] I. Gibson, D. Rosen, B. Stucker, (2015) Generalized Additive Manufacturing Process Chain. In: *Additive Manufacturing Technologies*. Springer, New York, NY. [https://doi.org/10.1007/978-1-4939-2113-3\\_3](https://doi.org/10.1007/978-1-4939-2113-3_3)
- [32] M. Mao, J. He, X. Li, B. Zhang, Q. Lei, Y. Liu, D. Li, (2017) The Emerging Frontiers and Applications of High-Resolution 3D Printing. *Micromachines*, 8, 113, <https://doi.org/10.3390/mi8040113>
- [33] S. Brahma & K. J. Rao & S. Shivashankar, (2010) Rapid growth of nanotubes and nanorods of wurtzite ZnO through microwave-irradiation of a metalorganic complex of zinc and a surfactant in solution, *Bulletin of Materials Science*, 33, pp. 89-95, 10.1007/s12034-010-0027-7
- [34] P.R. de S. Mendes, A.A. Aliche, R.L. Thompson, (2014) Parallel-plate Geometry Correction for

Transient Rheometric Experiments, *Appl. Rheol.* 24

- [35] Yang, B., Wei, C., Qian, F. et al., (2019) Surface Wettability Modulated by Surfactant and Its Effects on the Drug Release and Absorption of Fenofibrate Solid Dispersions. *AAPS PharmSciTech* 20, 234., <https://doi.org/10.1208/s12249-019-1446-4>
- [36] W.S. Janna, (2010) *Introduction to Fluid Mechanics*, 4th edition, 4th ed., CRC Press
- [37] E.P. Vrahopoulou, A.J. McHugh, (1987) Shear-thickening and structure formation in polymer solutions, *J. Nonnewton. Fluid Mech.*, doi:10.1016/0377-0257(87)85041-3.
- [38] Y. Guo, J. Xu, C. Yan, Y. Chen, X. Zhang, X. Jia, Y. Liu, X. Wang, F. Zhou, (2019) Direct Ink Writing of High Performance Architected Polyimides with Low Dimensional Shrinkage, *Adv. Eng. Mater.*, doi:10.1002/adem.201801314.
- [39] E. García-Tuñón, E. Feilden, H. Zheng, E. D'Elia, A. Leong, E. Saiz, (2017) Graphene Oxide: An All-in-One Processing Additive for 3D Printing, *ACS Appl. Mater. Interfaces.*, doi:10.1021/acsami.7b07717.
- [40] A.D. Valentine, T.A. Busbee, J.W. Boley, J.R. Raney, A. Chortos, A. Kotikian, J.D. Berrigan, M.F. Durstock, J.A. Lewis, (2017) Hybrid 3D Printing of Soft Electronics, *Adv. Mater.*, 1703817, doi:10.1002/adma.201703817.
- [41] N.J. Mewis, J. & Wagner, (2012) *Colloidal Suspension Rheology*, Cambridge Univ Press.
- [42] Y. Shao, R. Han, X. Quan, K. Niu, (2021) Study on ink flow of silicone rubber for direct ink writing, *Journal of Applied Polymer Science*, e50819. <https://doi.org/10.1002/app.50819>
- [43] H. Yuk, X. Zhao, (2018) A New 3D Printing Strategy by Harnessing Deformation, Instability, and Fracture of Viscoelastic Inks, *Adv. Mater.* 30, doi:10.1002/adma.201704028.
- [44] A. Goyal, A. Kumar, P.K. Patra, S. Mahendra, S. Tabatabaei, P.J.J. Alvarez, G. John, P.M. Ajayan, (2009) In situ synthesis of metal nanoparticle embedded free standing multifunctional PDMS films, *Macromol. Rapid Commun.* 30, 1116–1122. doi:10.1002/marc.200900174.
- [45] S. Noimark, R.J. Colchester, R.K. Poduval, E. Maneas, E.J. Alles, T. Zhao, E.Z. Zhang, M. Ashworth, E. Tsolaki, A.H. Chester, N. Latif, S. Bertazzo, A.L. David, S. Ourselin, P.C. Beard, I.P. Parkin, I. Papakonstantinou, A.E. Desjardins, (2018) Polydimethylsiloxane Composites for Optical Ultrasound Generation and Multimodality Imaging, *Adv. Funct. Mater.* 28, doi:10.1002/adfm.201704919.
- [46] B.C.K. Tee, A. Chortos, R.R. Dunn, G. Schwartz, E. Eason, Z. Bao, (2014) Tunable flexible pressure sensors using microstructured elastomer geometries for intuitive electronics, *Adv. Funct. Mater.* 24, 5427–5434. doi:10.1002/adfm.201400712.
- [47] S.W. Lee, S.S. Lee, (2008) Shrinkage ratio of PDMS and its alignment method for the wafer level

process, *Microsyst Technol* 14, 205–208

- [48] Y. Xia and G. M. Whitesides, (1998) Soft lithography, *Annual Review of Materials Science*, 28:1, 153-184

CRediT authorship contribution statement

**Saja Aabith:** Investigation, Methodology, Formal Analysis, Writing - Original Draft;

**Richard Caulfield:** Investigation, Validation, Formal Analysis, Writing - Original Draft;

**Omid Akhlaghi:** Investigation, Methodology, Writing - Review & Editing;

**Anastasia Papadopoulou:** Investigation, Methodology, Formal Analysis, Writing - Review & Editing;

**Shervanthi Homer-Vanniasinkam:** Writing - Review & Editing, Funding Acquisition Supervision;

**Manish K. Tiwari:** Conceptualisation, Formal Analysis, Writing - Review & Editing , Supervision, Funding Acquisition, Project Administration.

#### Declaration of Competing Interest

The authors declare that they have no known competing financial interests or personal relationships that could have appeared to influence the work reported in this paper.

The authors declare the following financial interests/personal relationships which may be considered as potential competing interests:

Manish K. Tiwari reports financial support was provided by Wellcome EPSRC Centre for Interventional and Surgical Sciences. Manish K. Tiwari reports financial support was provided by European Research Council (ERC) under the European Union's Horizon 2020 research and innovation programme under grant agreement no. 714712. Saja Aabith reports financial support was provided by EPSRC DTP studentship award.